

GeoHeight-Bench: Towards Height-Aware Multimodal Reasoning in Remote Sensing

Xuran Hu^{1,2}, Zhitong Xiong^{3*}, Zhongcheng Hong², Yifang Ban¹, Xiaoxiang Zhu³, and Wufan Zhao^{2**}

¹ KTH Royal Institute of Technology

² The Hong Kong University of Science and Technology (Guangzhou)

³ Technical University of Munich

Project page: <https://teriri1999.github.io/GeoHeight/>

Abstract. Current Large Multimodal Models (LMMs) in Earth Observation typically neglect the critical "vertical" dimension, limiting their reasoning capabilities in complex remote sensing geometries and disaster scenarios where physical spatial structures often outweigh planar visual textures. To bridge this gap, we introduce a comprehensive evaluation framework dedicated to height-aware remote sensing understanding. First, to overcome the severe scarcity of annotated data, we develop a scalable, VLM-driven data generation pipeline utilizing systematic prompt engineering and metadata extraction. This pipeline constructs two complementary benchmarks: GeoHeight-Bench for relative height analysis, and a more challenging GeoHeight-Bench+ for holistic, terrain-aware reasoning. Furthermore, to validate the necessity of height perception, we propose GeoHeightChat, the first height-aware remote sensing LMM baseline. Serving as a strong proof of concept, our baseline demonstrates that synergizing visual semantics with implicitly injected height geometric features effectively mitigates the "vertical blind spot", successfully unlocking a new paradigm of interactive height reasoning in existing optical models.

Keywords: large multimodal models · remote sensing · earth observation · height-aware reasoning

1 Introduction

In recent years, Large Multimodal Models (LMMs) [20, 27, 29] have garnered wide-spread attention and achieved remarkable success in the field of Remote Sensing (RS) [18, 45, 54]. By embedding and fusing complex and heterogeneous modalities, LMMs significantly enhance the interactivity of GeoAI systems, bridging the gap between multi-source observation data and human-centric reasoning [5, 39]. However, existing RS multimodal models primarily focus on traditional optical tasks, such as localization, attribution, and semantic understanding

* Corresponding author. Email: zhitong.xiong@tum.de

** Corresponding author. Email: wufanzhao@hkust-gz.edu.cn

(e.g., object detection and segmentation) [12, 58]. They fundamentally overlook a critical dimension of geospatial data: the height perspective [31, 40]. In real-world expert systems, such as flood simulation, landslide susceptibility assessment, and urban morphology analysis, the vertical spatial structure of the terrain is often more critical than visual features [15, 36, 37]. Existing models relying solely on optical RS images, semantic categories and other modality frequently fail in these physically-grounded reasoning scenarios [23, 51], indicating a significant shortfall in current LMMs regarding height comprehension.

To bridge this gap, the introduction of the vertical dimension is imperative. Benefiting from abundant remote sensing products, vertical scale information can be readily acquired from LiDAR or InSAR data [9, 44], such as Digital Elevation Models (DEM) and Digital Surface Models (DSM). Despite this, there is currently a severe scarcity of multimodal instruction-tuning datasets that effectively pair RS products with height information. Furthermore, comprehending complex geospatial structures requires reasoning across multiple granularities. Existing benchmarks lack a systematic evaluation framework that spans pixel-level (e.g., precise elevation retrieval), object-level (e.g., relative height relationships), and scene-level (e.g., overall terrain relief) dimensions. The abstract nature of height information, combined with the lack of large-scale, multi-granular benchmark datasets, poses a significant bottleneck for multimodal information fusion of LMMs in remote sensing domain.

To overcome these limitations and empower LMMs with vertical perception, we propose **GeoHeight-Bench** and its advanced extension, **GeoHeight-Bench+**. Rather than focusing on a single task, this two-tier benchmark suite systematically integrates optical RS information, object categories, normalized DSM, and DEM data. Specifically, utilizing Vision-Language Models (VLMs) [3] alongside automated metadata extraction and prompt engineering, we construct GeoHeight-Bench to focus on the surface morphology of objects (i.e., pixel-level elevation and object-level relative heights). To further push the boundaries of spatial reasoning, we introduce the more challenging GeoHeight-Bench+, which scales up to capture complex, scene-level terrain relief and macroscopic geospatial variations. This automated pipeline effectively addresses the prohibitive cost and strong reliance on expert knowledge traditionally required for RS data annotation, achieving efficient, high-quality, and scalable image-text instruction generation.

Finally, to demonstrate the potential of height-aware models in real-world reasoning, we propose the first height-aware RS LMM baseline, **GeoHeightChat**. Through a carefully designed two-stage training process comprising modal feature alignment and instruction fine-tuning [13, 20], GeoHeightChat successfully achieved multimodal fusion. It translates abstract height data into interactive reasoning capabilities, proving that introducing the vertical dimension unlocks a new paradigm for LMM understanding across fundamental morphology analysis and complex real-world terrain reasoning.

The main contributions of this paper are summarized as follows:

1. **A Height-Aware RS Benchmark Dataset:** We constructed the first large-scale multimodal benchmark dedicated to vertical perception in remote sensing, filling the gap in height-related GeoAI understanding. This dataset comprises **GeoHeight-Bench** for foundational surface morphology and height reasoning, alongside a more challenging **GeoHeight-Bench+** dedicated to complex, scene-level terrain relief.
2. **A Scalable VLM-Driven Annotation Pipeline:** Addressing the bottleneck of high annotation costs and the need for expert knowledge in Earth observation, we propose an automated, VLM-driven pipeline [3] for metadata extraction and prompt engineering, enabling low-cost, expert-level multimodal data generation.
3. **The First Height-Aware RS LMM Baseline:** We introduce GeoHeightChat, a multimodal model that achieves robust optical-height fusion through two-stage training process. Extensive experiments demonstrate its superior interactive reasoning capabilities across multi-granular height tasks, unlocking a new dimension for RS LMMs.

2 Related Work

Large Multimodal Models in Remote Sensing Early adaptations like GeoChat [18] successfully migrated LLaVA architectures to Earth Observation, enabling region-level reasoning via instruction tuning. To address single-modality limitations, EarthGPT [54] integrated Optical, SAR, and Infrared data, enhancing non-intuitive interpretation, while EarthGPT-X [53] further extended this to handle multi-source imagery flexibly. Recently, foundation models have surged, SkySense [11] utilizes factorized spatiotemporal encoders, and its V2 variant [55] scales to billion-level parameters with Mixture-of-Experts (MoE) strategies, achieving state-of-the-art performance across diverse tasks. Other emerging models like GeoRSMLLM [56] and generalized frameworks surveyed in [21, 48] demonstrate the rapid evolution towards universal perception. Despite these advancements in visual semantic understanding [42], existing RS-LMMs generally lack explicit modeling of vertical geometric structures, resulting in a "vertical blind spot" in complex remote sensing scenarios.

Reasoning Segmentation and Agents Reasoning segmentation extends LMMs from bounding boxes to pixel-level understanding. The pioneering LISA paradigm [20] introduced the "embedding-as-mask" strategy, which GSVA [47] generalized to multimodal contexts. In the geospatial domain, SegEarth-R1 [22] and SegEarth-R2 [49] adapted this by incorporating spatial attention supervision and dynamic query mechanisms to handle scale variations and multi-target instructions. Similarly, LISAt [33] leveraged large-scale synthesized data (GRES [26]) to unlock fine-grained geospatial reasoning. Further advancements like GeoPixel [38] and OmniRIS [14] pushed towards pixel grounding and omni-prompting for complex referring expressions. However, these methods primarily focus on se-

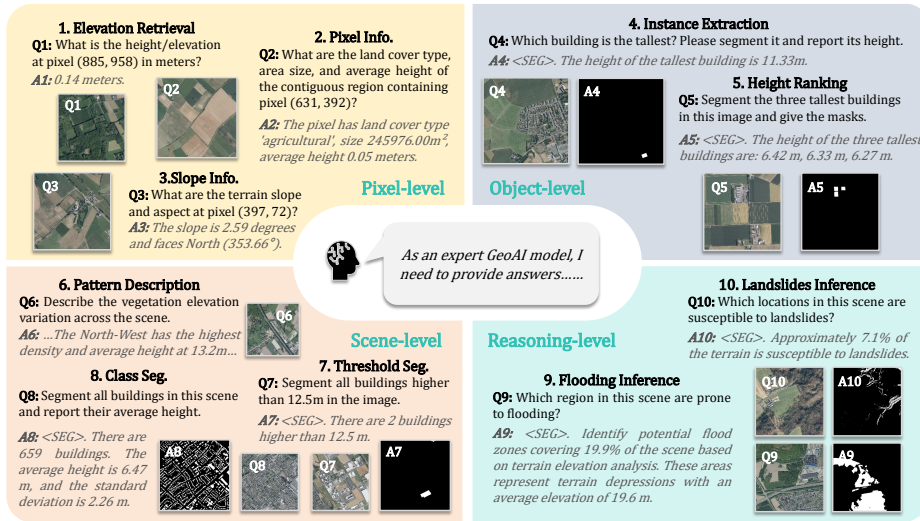


Fig. 1: Overview of the GeoHeight-Bench (+). We construct a comprehensive benchmark comprising 10 diverse tasks organized into four hierarchical levels: Pixel-level retrieval, Object-level extraction, Scene-level analysis, and Reasoning-level inference.

mantic attributes rather than geometric properties, limiting their utility in some specific scenarios.

Remote Sensing Benchmarks and Height Perception Evaluating LMMs in remote sensing requires comprehensive benchmarks. UrBench [58] integrated multi-view data (satellite and street view) for cross-view reasoning. Other efforts like the Vision-Centric Benchmark [2] focus on general visual tasks but lack depth. While covering horizontal spatial reasoning, these benchmarks overlook the critical vertical dimension. Traditional vertical perception relies on explicit height products or domain adaptation [41]. Recent works like HATFormer [25] and PARIS3D [16] have attempted to encode height into Transformers for 3D change detection or part segmentation. However, there is no unified benchmark evaluating implicit height reasoning solely from optical imagery, a gap our GeoHeight-Bench aims to fill.

3 GeoHeight-Bench

3.1 Benchmark Tasks

We introduce the GeoHeight-Bench and GeoHeight-Bench+ to comprehensively evaluate LMMs in remote sensing height-related reasoning through ten distinct tasks across four dimensions, aiming to assess the models' height perception and spatial reasoning capabilities. Figure 1 illustrates the task types in our benchmark; further details are provided in the Supplementary Materials.

The GeoHeight-Bench comprises tasks organized into three hierarchical levels: Pixel-level, Object-level, and Scene-level. GeoHeight-Bench+ additionally incorporates Reasoning-level tasks, designed specifically for assessing terrain-related questions.

1. **Pixel-level** encompasses three tasks: Elevation Retrieval (ER), Pixel Info. (PI), and Slope Info. (SI). ER queries specific coordinates within the scene to acquire height information. PI integrates semantic, height, and scale perception to comprehensively measure LMM performance. SI, exclusive to GeoHeight+, calculates the terrain slope and aspect at a given coordinate.
2. **Object-level** includes two tasks: Instance Extraction (IE) and Height Ranking (HR). IE need to identify instances within a specific category; unlike standard VQA, the model must output both the elevation information and the segmentation mask for the specified instance. HR introduces sorting tasks and complex reasoning, requiring the model to rank buildings in the scene by height and return their corresponding masks.
3. **Scene-level** evaluates the LMMs’ capacity for global information capture and natural language description. It contains three tasks: Pattern Description (PD), Threshold Seg. (TS), and Class Seg. (CS). PD describes the height distribution of land-cover categories within the remote sensing imagery, or slope information (exclusive to GeoHeight+). TS challenges the model to segment instances exceeding a given elevation threshold, simulating conditional retrieval in scenarios such as disaster management. CS requires the model to macroscopically summarize specific categories within the scene, extracting global statistical information and masks.
4. **Reasoning-level** consists of two tasks: Landslides Inference (LI) and Flooding Inference (FI). By integrating terrain information and land-cover categories, we designed two types of visual question answering directly correlated with height information, rigorously evaluating the models’ reasoning capabilities in complex scenarios.

3.2 Benchmark Pipeline

The construction of the GeoHeight-Bench follows a systematic pipeline comprising three main stages: attribute extraction, prompt design & LLM reasoning, and human verification. Each stage incrementally refines the data representation to ensure completeness, consistency, and semantic accuracy across modalities. The overall workflow of the benchmark construction is shown in Figure 2.

Data Collection and Attribute Extraction: Although large vision-language models have demonstrated impressive cross-modal reasoning abilities, they remain limited in accurately perceiving fine-grained spatial cues and quantitative elevation patterns inherent in remote sensing imagery. To mitigate this, we designed an algorithmic extraction module to construct structured, model-readable metadata from raw data sources. Specifically, we employ the GeoNRW [4], RSMSS [50], and FLAIR [19] datasets, and integrate official DTM data of

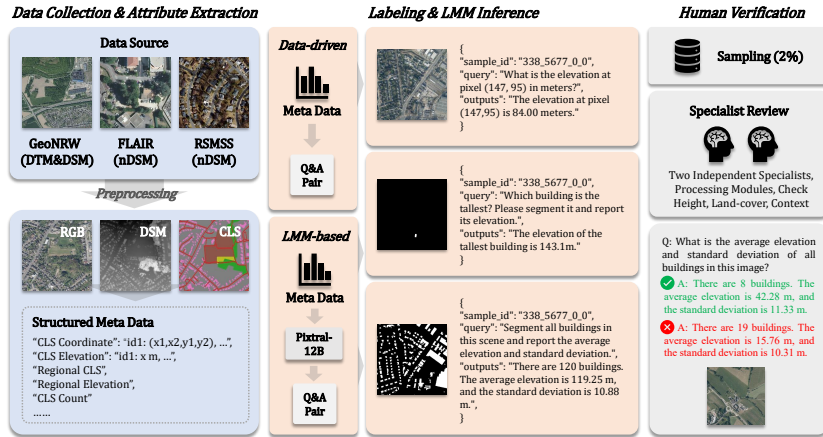


Fig. 2: Pipeline of the GeoHeight-Bench generation and verification.

NRW products, as the foundation for the GeoHeight-Bench. We first perform preliminary semantic filtering by referencing land-cover classification maps and considering connectivity to identify coherent land-cover regions. For each region, we compute descriptive statistics, including the mean of elevation/height, and merge these attributes into unified metadata to capture both categorical semantics and height-related structural context. Furthermore, task-specific filtering strategies are applied to reduce the interference of redundant information on LMM reasoning. For some information retrieval tasks, we do not use LLM reasoning but directly extract information from metadata and embed answer templates.

Prompt Design and LMM Inference: Based on the extracted meta-frames, we construct a two-tier prompt schema inspired by recent work in multimodal instruction tuning [8, 43]. The system prompt defines global constraints, instructing the model to produce precise and unambiguous responses while adhering to scientific language conventions. The user prompt, in contrast, encodes task-specific instructions such as identifying the highest object within a scene, comparing elevation gradients, or reasoning about object-terrain interactions.

We adopt Pixtral-12B [3] as the vision-language reasoning backbone. Its 12-billion-parameter architecture combines lightweight visual adapters and a cross-attention language core, enabling efficient multimodal reasoning under limited GPU resources. During QA generation, we employ iterative self-consistency checking: the model is prompted multiple times under varying linguistic formulations, and inconsistent responses are automatically filtered through semantic matching. The remaining answers are post-processed to remove uncertain or underspecified phrases (e.g., "possibly," "it seems") and normalized into a consistent syntactic structure, forming the final VQA pairs.

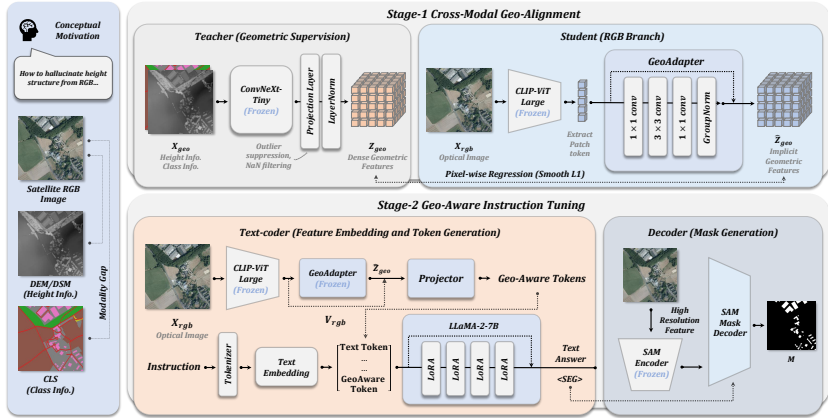


Fig. 3: The proposed GeiHeightChat framework comprises two training stages: Cross-Modal Geo-Alignment and Geo-Aware Instruction Tuning.

Human Verification: While automated inference ensures scalability, high-quality benchmarks in scientific domains demand rigorous validation [31, 46]. We therefore integrate a human-in-the-loop verification stage to guarantee the accuracy and interpretability of the generated annotations. We extract a 2% sample of the total data for validation, where each QA pair is independently reviewed by at least two remote sensing specialists, who verify the correctness of height descriptions, land-cover interpretations, and contextual reasoning. Additionally, we employ random stratified sampling for secondary quality auditing to estimate annotation precision and inter-rater agreement. After this multi-round verification, no major inconsistencies or conceptual errors were found, confirming the benchmark’s reliability and readiness for large-scale evaluation.

4 GeoHeightChat

This section presents GeoHeightChat, the first LMM equipped with "vertical perspective", which achieves question answering and segmentation via implicit geospatial understanding. The core of our approach lies in bridging the modality gap between optical remote sensing imagery and geospatial information (e.g., elevation, terrain), thereby enabling the inference process to rely solely on optical images. Specifically, we employ a two-stage training paradigm consisting of: (1) Cross-Modal Geo-Alignment, and (2) Geo-Aware Instruction Tuning.

4.1 Problem Formulation

Let $\mathcal{D} = \{(X_{rgb}^i, X_{geo}^i, T_{inst}^i, T_{gt}^i, M_{gt}^i)\}_{i=1}^N$ denote a dataset containing N samples. Here, $X_{rgb} \in \mathbb{R}^{H \times W \times 3}$ represents the high-resolution optical satellite imagery. $X_{geo} \in \mathbb{R}^{H \times W \times C_{geo}}$ represents the auxiliary geospatial data (where $C_{geo} \in$

$\{2, 3\}$ corresponds to height information and semantic maps). T_{inst} is the language instruction, T_{gt}^i is the corresponding ground-truth answer, and $M_{gt} \in \{0, 1\}^{H \times W}$ is the binary ground-truth segmentation mask.

Our goal is to learn a mapping function $\mathcal{F}_\theta : (X_{rgb}, T_{inst}) \rightarrow (\hat{M}, \hat{T})$, where \hat{M} and \hat{T} are the predicted mask and answer. Crucially, while X_{geo} is only available during the training of the alignment module (Stage 1), it is unavailable during the inference process. The model must implicitly infer the geometric features \mathcal{Z}_{geo} solely from X_{rgb} to support complex reasoning tasks that typically require explicit height information.

4.2 Architecture Overview

The GeoHeightChat architecture is built upon LISA-7B [20], extended with our GeoEncoder and GeoAdapter. The framework consists of five main components:

1. **Vision Backbone (\mathcal{V}):** We employ the pretrained CLIP ViT-Large [34] as the visual encoder. Given an RGB image X_{rgb} , it extracts semantic visual features $\mathbf{V}_{rgb} = \mathcal{V}(X_{rgb})$, where $\mathbf{V}_{rgb} \in \mathbb{R}^{L \times D_v}$.
2. **GeoEncoder (\mathcal{G}):** Serving as the geometric teacher, we utilize a frozen ConvNeXt-Tiny backbone [30] initialized with ImageNet weights. It processes the auxiliary geospatial data X_{geo} (e.g., Elevation and Semantic Maps) to extract dense structural embeddings $\mathbf{Z}_{real} = \mathcal{G}(X_{geo})$. This module provides the explicit geometric supervision signals for aligning the RGB features.
3. **GeoAdapter (\mathcal{A}):** A lightweight, trainable module designed to project optical visual features into a geometry-aware latent space. It transforms \mathbf{V}_{rgb} into implicit geometric features $\hat{\mathbf{Z}}_{geo} = \mathcal{A}(\mathbf{V}_{rgb})$. Structurally, the GeoAdapter consists of a sequence of ResNet Bottleneck blocks to preserve high-frequency details essential for dense prediction tasks.
4. **Large Language Model (\mathcal{L}):** Following LISA-7B, we utilize Llama-2-7B [43] as the reasoning core. To enable efficient fine-tuning, we inject LoRA modules [13] into the query (W_q) and value (W_v) projections of the Transformer attention blocks. The LLM processes the multimodal sequence of text embeddings and visual embeddings to generate a response text and a special token [SEG].
5. **Visual Encoder (\mathcal{E}_v) and Mask Decoder (\mathcal{D}_{mask}):** Following LISA, we adopt the Segment Anything Model (SAM) [17] encoder and decoder. The visual encoder (\mathcal{E}_v) captures fine-grained spatial features, and the decoder (\mathcal{D}_{mask}) takes the embedding of the [SEG] token as a prompt (along with the visual feature maps) to generate the binary mask \hat{M} .

4.3 Cross-Modal Geo-Alignment

The primary goal of this stage is to train a lightweight adapter that can translate visual features from a frozen CLIP encoder into a geometry-aware feature space defined by a geometric teacher. Unlike contrastive approaches that learn

global semantic alignment, we adopt a dense feature distillation paradigm to rigorously preserve both the semantic direction and the activation magnitude of the geospatial features for precise dense prediction.

The Teacher: GeoEncoder. We employ a ConvNeXt-Tiny backbone initialized with ImageNet weights as the geometric teacher \mathcal{G} . The input to the teacher consists strictly of geospatial data X_{geo} . To adapt the pre-trained backbone to 2/3-channel geo-data, we append a zero-filled channel to X_{geo} before processing. The teacher extracts hierarchical geometric features, which are then projected and normalized to form the regression targets:

$$\mathbf{Z}_{real} = \text{LayerNorm}(\text{Proj}(\mathcal{G}(X_{geo}))) \quad (1)$$

where $\mathbf{Z}_{real} \in \mathbb{R}^{N \times D}$ represents the dense geometric embeddings. To ensure numerical stability during regression, we apply explicit outlier suppression to \mathbf{Z}_{real} by clamping values within a robust range.

The Student: GeoAdapter. The student branch processes the RGB image X_{rgb} using a frozen CLIP ViT-Large encoder. We extract the patch tokens \mathbf{V}_{rgb} from the penultimate layer. The core component, GeoAdapter (\mathcal{A}), is designed as a stack of Bottleneck Residual Blocks. Each block consists of:

$$\text{Block}(\mathbf{x}) = \mathbf{x} + \gamma \cdot \mathcal{F}_{conv}(\text{GroupNorm}(\mathbf{x})) \quad (2)$$

where \mathcal{F}_{conv} denotes the bottleneck sequence. Crucially, we employ a Zero-Initialization strategy for the learnable scaling factor γ (initialized to 0). This ensures that the GeoAdapter acts as an identity function at the start of training, preserving the semantic integrity of CLIP features while gradually learning geometric shifts.

Distillation Objective: We formulate the alignment as a regression problem. The objective is to minimize the reconstruction error between the hallucinated features $\hat{\mathbf{Z}}_{geo} = \mathcal{A}(\mathbf{V}_{rgb})$ and the teacher’s features \mathbf{Z}_{real} . We utilize the Smooth L1 Loss [10] to be robust against outliers in the geospatial data:

$$\mathcal{L}_{align} = \frac{1}{N} \sum_{i=1}^N \text{SmoothL1}(\hat{\mathbf{z}}_i, \mathbf{z}_i^{real}) \quad (3)$$

where $\hat{\mathbf{z}}_i$ and \mathbf{z}_i^{real} denote the feature vectors at spatial location i . This forces the adapter to infer explicit height and semantic structures solely from RGB texture cues.

4.4 Geo-Aware Instruction Tuning

In the second stage, we integrate the pre-trained GeoAdapter into the LISA framework for end-to-end segmentation.

Geo-Aware Adapter Integration: To preserve the learned geometric alignment, we freeze both the CLIP encoder and the GeoAdapter. The aligned features $\hat{\mathbf{Z}}_{geo}$ act as a “structural prior” and are fused with the standard visual

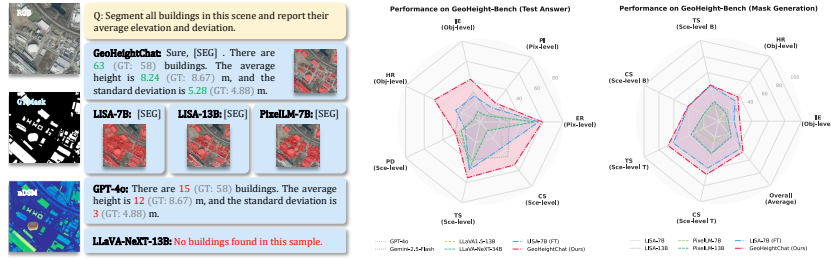


Fig. 4: Comparison between GeoHeightChat and LLMs.

features \mathbf{V}_{rgb} via the projector \mathcal{P} to form Geo-Aware tokens H_v :

$$H_v = \mathcal{P}(\mathbf{V}_{rgb} + \lambda \cdot \hat{\mathbf{Z}}_{geo}) \quad (4)$$

where λ is a learnable scalar balancing texture and geometry. These tokens are concatenated with text instructions to fine-tune the LLM. Following LISA, we employ LoRA for efficient fine-tuning of the LLM and update the SAM mask decoder, while keeping other components frozen.

Geometric Reasoning Inference: During inference, the model operates in a purely RGB mode. The input X_{rgb} passes through the frozen GeoAdapter, which injects the learned structural priors (e.g., relative height) into the LLM. This allows GeoHeightChat to correctly interpret complex instructions like "Segment the building with the highest elevation" by leveraging latent geometric features, even without explicit height data.

Training Objectives: The total objective \mathcal{L}_{total} is a weighted sum of the autoregressive text generation loss (\mathcal{L}_{txt}) and the segmentation mask loss (\mathcal{L}_{mask}):

$$\mathcal{L}_{total} = \lambda_{txt} \mathcal{L}_{txt} + \lambda_{mask} (\mathcal{L}_{bce} + \mathcal{L}_{dice}) \quad (5)$$

where \mathcal{L}_{txt} is the cross-entropy loss for next-token prediction, and \mathcal{L}_{mask} combines Binary Cross-Entropy and Dice loss [32] to supervise the SAM decoder predictions against ground truth masks M_{gt} . By optimizing this objective, the LoRA modules learn to interpret geometric cues provided by the GeoAdapter to steer the segmentation.

5 Experimental Results

In this section, we comprehensively evaluate various LLMs on the GeoHeight-Bench to compare the performance of existing models with our proposed GeoHeightChat on height-aware and spatial reasoning tasks.

5.1 Experiment Setting

Compared Models. To ensure a comprehensive evaluation, we select 2 closed-source models and 11 open-source LLMs for comparison on the GeoHeight-

Table 1: Quantitative results of text generation and spatial reasoning on the GeoHeight-Bench. The best and second-best results are highlighted in **bold** and underlined, respectively.

Model	Pix-level		Obj-level		Sce-level			Overall
	ER	PI	IE	HR	PD	TS	CS	
<i>Closed-source LMMs</i>								
GPT-4o	19.40	7.02	12.20	8.18	24.89	45.34	34.23	21.61
Gemini-2.5-Flash	28.11	11.45	<u>29.82</u>	22.57	<u>27.11</u>	37.30	<u>42.74</u>	28.45
<i>Open-source LMMs</i>								
InternVL2-2B	17.78	5.77	18.80	5.27	15.75	39.19	10.94	16.22
InternVL2-4B	12.22	10.27	22.00	7.75	21.90	46.44	34.04	22.09
InternVL2-8B	14.01	3.90	13.51	5.41	17.06	32.62	38.63	17.88
LLaVA1.5-7B	36.72	9.00	7.83	5.41	27.59	44.73	10.03	20.19
LLaVA1.5-13B	53.46	9.48	7.07	5.14	22.96	40.76	10.25	21.30
LLaVA-NeXT-7B-Mistral	22.78	1.97	7.18	5.78	19.33	44.99	10.76	16.11
LLaVA-NeXT-7B-Vicuna	34.07	9.16	9.63	5.83	18.06	44.54	10.12	18.78
LLaVA-NeXT-13B	55.64	9.48	9.27	7.33	20.40	44.98	10.42	22.50
LLaVA-NeXT-34B	51.37	7.85	10.43	6.53	20.17	45.84	11.00	21.88
Ministral3-8B	17.67	6.17	5.28	4.05	15.77	33.14	8.15	12.89
Pixtral-12B	30.60	7.77	9.71	5.52	20.17	40.30	12.23	18.04
<i>Height-aware LMMs</i>								
LISA-7B (FT)	<u>56.58</u>	<u>17.53</u>	25.75	<u>26.25</u>	16.12	<u>47.54</u>	32.31	<u>31.73</u>
GeoHeightChat	59.98	23.36	42.19	49.09	26.16	55.24	52.97	44.14

Bench (+), along with 4 multimodal reasoning segmentation models. The closed-source models include GPT-4o [1] and Gemini-2.5-Flash [7]. The open-source large multimodal models encompass the InternVL series [6], LLaVA series [27], LLaVA-NeXT series [28], as well as Ministral and Pixtral models [3, 24]. For the mask generation task, we benchmark against the LISA [20] and PixelLM series [35]. Additionally, to validate the effectiveness of explicitly introducing geospatial information, we fine-tune the LISA-7B model (denoted as LISA-7B FT) by concatenating optical, height, and categorical information into a three-channel input, serving as another baseline.

Evaluation Strategy. We establish a standardized response processing pipeline for different task settings. For template-based QA, to ensure objective evaluation, we utilize Qwen2.5-1.5B [52] for post-processing extraction and set a numerical error threshold of 20%; predictions falling within this range are deemed correct. For open-ended questions, we employ the Qwen2.5-7B as a judge model to assess semantic accuracy and logical quality [52, 57]. For the mask generation task, following existing semantic segmentation research, we adopt mean Intersection over Union (mIoU) and cumulative Intersection over Union (cIoU) as our core evaluation metrics. Detailed evaluation protocols and prompt settings are provided in the Supplementary Materials.

5.2 Main Results

Results on GeoHeight-Bench. As shown in Table 1 and Figure 4, GeoHeightChat achieves an overall accuracy of 44.14% on GeoHeight-Bench (text

Table 2: Quantitative results of text generation on the GeoHeight-Bench+.

Model	Pix-level			Obj-level		Sce-level			Overall
	ER	PI	SI	IE	HR	PD	TS	CS	
<i>Closed-source LMMs</i>									
GPT-4o	0.00	0.68	15.03	6.01	5.74	29.05	38.51	25.90	15.12
Gemini-2.5-Flash	2.70	5.41	14.86	5.71	10.03	20.04	<u>45.95</u>	35.14	17.48
<i>Open-source LMMs</i>									
InternVL2-2B	0.68	0.56	14.18	7.07	6.41	15.52	37.33	13.51	11.91
InternVL2-4B	5.41	16.58	10.14	7.42	8.20	20.29	38.34	33.61	17.50
InternVL2-8B	1.01	1.80	14.53	6.71	5.74	12.09	37.67	35.08	14.33
LLaVA1.5-7B	5.07	10.26	16.05	6.36	5.78	23.91	38.01	11.66	14.64
LLaVA1.5-13B	9.12	11.50	15.88	6.01	6.35	23.78	31.42	17.12	15.15
LLaVA-NeXT-7B-Mistral	2.27	0.00	14.86	6.07	4.62	16.63	38.01	11.82	11.79
LLaVA-NeXT-7B-Vicuna	7.43	10.59	16.39	7.77	5.06	18.08	37.82	11.88	14.38
LLaVA-NeXT-13B	7.09	12.62	15.54	6.71	5.93	12.99	38.07	12.44	13.92
LLaVA-NeXT-34B	11.32	11.38	15.24	7.27	6.20	19.76	37.91	14.26	15.42
Ministral3-8B	8.60	2.01	12.77	5.26	4.87	13.64	37.75	11.73	12.08
Pixtral-12B	10.75	2.96	14.60	5.34	5.29	15.11	37.60	12.98	13.08
<i>Height-aware LMMs</i>									
LISA-7B (FT)	<u>42.76</u>	<u>40.03</u>	18.96	<u>48.74</u>	<u>39.60</u>	<u>31.06</u>	43.11	<u>61.29</u>	<u>40.69</u>
GeoHeightChat	76.35	52.62	<u>18.58</u>	97.53	94.87	48.48	55.41	80.91	65.59

tasks), significantly outperforming existing optical LMMs such as GPT-4o (21.61%) and Gemini-2.5-Flash (28.45%). Notably, GeoHeightChat demonstrates an overwhelming advantage in Pixel-level and Object-level tasks, attaining accuracies of 59.98% and 49.09% in Elevation Retrieval and Height Ranking tasks, respectively, which robustly validates the effectiveness of the injected height priors. Regarding fine-grained mask generation (Table 3), our proposed baseline achieves 37.58% and 47.09% in mIoU and cIoU, surpassing existing multimodal segmentation models. Furthermore, although the LISA-7B (FT) shows improved segmentation performance, it still underperforms GeoHeightChat. This implicitly confirms that our implicit height feature alignment strategy is more effective than simple channel concatenation in enhancing the model’s "vertical perception".

Results on GeoHeight-Bench+. We furthermore conduct experiments on the more challenging GeoHeight-Bench+ (which introduces complex geological attributes such as terrain relief and slope) to evaluate the models’ advanced reasoning capabilities under global terrain perception. As shown in Table 2, GeoHeightChat takes the lead with an overall score of 65.59%, not only widening the gap with closed-source models but also significantly outperforming 30-billion-parameter-class open-source models like LLaVA-NeXT-34B. This advantage is particularly prominent in Reasoning-level tasks, fully demonstrating that implicitly aligning height information can effectively unlock the advanced reasoning capabilities required to parse complex spatial topographic variations. The segmentation results in Table 4 present a similar trend, GeoHeightChat also outperformed in mask output precision and robustness.

Table 3: Fine-grained mask generation on the GeoHeight-Bench, evaluated by mIoU and cIoU. Scene-level calculations were performed on building(B) and tree(T).

Model	Obj-level		Sce-level(B)		Sce-level(T)		Overall
	IE	HR	TS	CS	TS	CS	
<i>Metrics - mIoU</i>							
LISA-7B	6.20	12.91	18.75	12.30	23.20	33.88	17.87
LISA-13B	10.24	15.96	19.97	14.22	30.64	33.77	20.80
PixelLM-7B	8.84	9.55	18.02	11.64	23.64	15.82	14.58
PixelLM-13B	11.36	14.42	20.22	12.29	34.88	32.44	20.94
LISA-7B (FT)	<u>13.35</u>	<u>26.45</u>	30.77	<u>28.76</u>	<u>53.41</u>	<u>44.06</u>	<u>32.80</u>
GeoHeightChat	16.03	31.23	<u>30.23</u>	33.14	62.04	52.83	37.58
<i>Metrics - cIoU</i>							
LISA-7B	8.09	13.71	21.60	16.13	26.34	41.79	21.28
LISA-13B	11.62	17.45	21.99	20.34	33.73	40.86	24.34
PixelLM-7B	9.00	6.76	19.47	18.03	28.03	25.12	17.73
PixelLM-13B	11.86	13.52	24.46	19.70	36.76	39.56	24.31
LISA-7B (FT)	<u>18.81</u>	<u>31.51</u>	<u>44.23</u>	<u>40.58</u>	<u>60.72</u>	<u>58.11</u>	<u>42.33</u>
GeoHeightChat	25.52	37.33	44.76	41.03	67.88	66.02	47.09

5.3 Ablation Study

To validate the core designs of GeoHeightChat, we conduct ablation studies on GeoHeight-Bench (Table 5), evaluating geometric supervision modalities (Stage-1) and feature fusion strategies (Stage-2).

Impact of Teacher Supervision Modalities. As shown in Table 5, the baseline lacking geospatial alignment struggles significantly (12.58%). Supervising the GeoAdapter solely with height information yields a massive performance leap (35.11%), demonstrating successful hallucination of vertical geometry. Conversely, using only semantic maps provides categorical boundaries but lacks height-related context, leading to suboptimal reasoning (23.68%). Combining both modalities achieves the best results, proving that height data supplies essential vertical scale while semantic maps offer crucial boundary constraints for precise dense prediction.

Effectiveness of the Feature Fusion Strategy. To integrate hallucinated geometric features without overwhelming the LLM’s pre-trained knowledge, we compare our adaptive residual connection ($\mathcal{P}(V_{rgb} + \lambda \cdot \hat{Z}_{geo})$) against standard channel-wise concatenation ($\mathcal{P}([V_{rgb}, \hat{Z}_{geo}])$). The adaptive approach consistently outperforms concatenation across all metrics (e.g., boosting Overall accuracy from 33.92% to 42.94%, and mIoU from 28.58% to 37.58%). The learnable scalar λ dynamically balances visual textures and geometric priors, effectively preventing the injected geometry from washing out fundamental visual semantics.

5.4 Discussion

Attribution of LMMs’ Performance. Existing LMMs excel in category-recognition and counting (TS, CS) but struggle with height-perception and localization (ER, IE), exhibiting severe numerical drift and localization failures (Table

Table 4: Fine-grained mask generation results on the GeoHeight-Bench+, evaluated by mIoU and cIoU. Scene-level calculations were performed on building(B) and tree(T).

Model	Obj-level		Sce-level(B)		Sce-level(T)		Res-level		Overall
	IE	HR	TS	CS	TS	CS	LI	FI	
<i>Metrics - mIoU</i>									
LISA-7B	1.69	3.75	14.10	18.70	19.88	30.40	0.32	3.44	11.54
LISA-13B	2.49	4.48	12.73	20.63	17.98	28.18	1.32	<u>5.28</u>	11.64
PixelLM-7B	1.26	3.11	12.40	19.01	18.87	24.02	12.16	0.01	11.36
PixelLM-13B	1.64	3.63	12.84	20.16	18.51	25.58	8.55	0.00	11.36
LISA-7B (FT)	<u>6.22</u>	<u>8.29</u>	<u>20.89</u>	<u>28.65</u>	<u>47.95</u>	<u>40.04</u>	<u>17.92</u>	4.87	<u>21.85</u>
GeoHeightChat	7.76	14.59	27.56	30.93	54.08	53.94	30.63	6.57	28.26
<i>Metrics - cIoU</i>									
LISA-7B	3.36	3.38	14.42	24.58	21.27	37.38	0.51	4.04	13.62
LISA-13B	3.66	4.32	12.09	29.27	18.67	34.50	1.68	<u>5.77</u>	13.75
PixelLM-7B	1.81	1.92	12.12	18.11	19.64	25.16	10.74	0.01	11.69
PixelLM-13B	1.58	1.49	12.91	30.94	19.19	27.38	10.43	0.00	12.99
LISA-7B (FT)	<u>7.90</u>	<u>10.03</u>	<u>28.66</u>	<u>43.44</u>	<u>51.08</u>	<u>58.22</u>	<u>15.09</u>	4.98	<u>27.43</u>
GeoHeightChat	9.37	16.44	40.66	52.59	58.76	75.60	28.71	6.40	36.07

Table 5: Ablation study of the core designs on the GeoHeightChat. Here reports the text accuracy alongside mask generation metrics (mIoU and cIoU).

Model Variants	Modality		Fusion Strategy	Text Acc.	Mask Acc.		Overall
	Height	Class			mIoU	cIoU	
Baseline (No Geo-Align)	\times	\times	-	-	11.54	13.62	12.58
Height Only	\checkmark	\times	Adapt. Res.	36.32	<u>30.95</u>	<u>38.07</u>	<u>35.11</u>
Class Only	\times	\checkmark	Adapt. Res.	31.84	18.44	20.76	23.68
Concat Fusion	\checkmark	\checkmark	Concat.	<u>40.87</u>	28.58	32.30	33.92
GeoHeightChat	\checkmark	\checkmark	Adapt. Res.	44.14	37.58	47.09	42.94

1). This trend also extends to segmentation, where CS mask quality consistently outpaces Pixel- and Object-level tasks. Evidently, current LMMs over-rely on visual semantic features and lack an intrinsic grasp of absolute physical scale, necessitating future integration of height-annotated multimodal datasets.

The ‘‘Vertical Blind Spot’’ of Optical Models. Cutting-edge models excel in visual semantics but fail in height-related scenarios. In Tables 2 and 4, pure optical baselines (e.g., PixelLM) score near zero on Landslide and Flood Inference tasks, as planar RGB textures cannot model topography. By implicitly injecting height priors, GeoHeightChat achieves a qualitative leap (e.g., 28.71% cIoU on LI), demonstrating that vertical spatial perception is indispensable for reliable real world application.

6 Conclusions

In this work, we introduced GeoHeight-Bench to address the ‘‘vertical blind spot’’ in current remote sensing LMMs. Through an efficient, VLM-driven data generation pipeline, we constructed two comprehensive benchmarks, GeoHeight-Bench

and GeoHeight-Bench+, to evaluate height-aware reasoning. Furthermore, we proposed GeoHeightChat, the first height-aware remote sensing LMM baseline. By employing a two-stage training paradigm and a lightweight GeoAdapter, our model successfully bridges the modality gap, implicitly inferring vertical geometry from purely optical remote sensing inputs. Extensive experiments validate that GeoHeightChat achieves good performance across both text and mask generation tasks. By explicitly unlocking the third dimension in LMM reasoning, our work paves the way for more robust AI systems in RS morphology analysis and application.

References

1. Achiam, J., Adler, S., Agarwal, S., Ahmad, L., Akkaya, I., Aleman, F.L., Almeida, D., Altenschmidt, J., Altman, S., Anadkat, S., et al.: Gpt-4 technical report. arXiv preprint arXiv:2303.08774 (2023) **11**
2. Adejumo, A., Yeganli, F., Broni-bediako, C., Xiao, A., Yokoya, N., Siam, M.: A vision centric remote sensing benchmark. arXiv preprint arXiv:2503.15816 (2025) **4**
3. Agrawal, P., Antoniak, S., Hanna, E.B., Bout, B., Chaplot, D., Chudnovsky, J., Costa, D., De Monicault, B., Garg, S., Gervet, T., et al.: Pixtral 12b. arXiv preprint arXiv:2410.07073 (2024) **2, 3, 6, 11**
4. Baier, G., Deschemps, A., Schmitt, M., Yokoya, N.: Geonrw (2020). <https://doi.org/10.21227/s5xq-b822>, <https://dx.doi.org/10.21227/s5xq-b822> **5**
5. Bazi, Y., Bashmal, L., Al Rahhal, M.M., Ricci, R., Melgani, F.: Rs-llava: A large vision-language model for joint captioning and question answering in remote sensing imagery. *Remote Sensing* **16**(9), 1477 (2024) **1**
6. Chen, Z., Wu, J., Wang, W., Su, W., Chen, G., Xing, S., Zhong, M., Zhang, Q., Zhu, X., Lu, L., et al.: Internvl: Scaling up vision foundation models and aligning for generic visual-linguistic tasks. In: Proceedings of the IEEE/CVF conference on computer vision and pattern recognition. pp. 24185–24198 (2024) **11**
7. Comanici, G., Bieber, E., Schaekermann, M., Pasupat, I., Sachdeva, N., Dhillon, I., Blistein, M., Ram, O., Zhang, D., Rosen, E., et al.: Gemini 2.5: Pushing the frontier with advanced reasoning, multimodality, long context, and next generation agentic capabilities. arXiv preprint arXiv:2507.06261 (2025) **11**
8. Dai, W., Li, J., Li, D., Tiong, A., Zhao, J., Wang, W., Li, B., Fung, P.N., Hoi, S.: Instructblip: Towards general-purpose vision-language models with instruction tuning. *Advances in neural information processing systems* **36**, 49250–49267 (2023) **6**
9. Farr, T.G., Rosen, P.A., Caro, E., Crippen, R., Duren, R., Hensley, S., Kobrick, M., Paller, M., Rodriguez, E., Roth, L., et al.: The shuttle radar topography mission. *Reviews of geophysics* **45**(2) (2007) **2**
10. Girshick, R.: Fast r-cnn. In: Proceedings of the IEEE international conference on computer vision. pp. 1440–1448 (2015) **9**
11. Guo, X., Lao, J., Dang, B., Zhang, Y., Yu, L., Ru, L., Zhong, L., Huang, Z., Wu, K., Hu, D., et al.: Skysense: A multi-modal remote sensing foundation model towards universal interpretation for earth observation imagery. In: Proceedings of the IEEE/CVF Conference on Computer Vision and Pattern Recognition. pp. 27672–27683 (2024) **3**

12. Hao, X., Chen, W., Yan, Y., Zhong, S., Wang, K., Wen, Q., Liang, Y.: Urban-*vlp*: Multi-granularity vision-language pretraining for urban socioeconomic indicator prediction. In: Proceedings of the AAAI Conference on Artificial Intelligence. vol. 39, pp. 28061–28069 (2025) [2](#)
13. Hu, E.J., Shen, Y., Wallis, P., Allen-Zhu, Z., Li, Y., Wang, S., Wang, L., Chen, W., et al.: Lora: Low-rank adaptation of large language models. *ICLR* **1**(2), 3 (2022) [2](#), [8](#)
14. Hu, Y., Wang, Q., Shao, W., Xie, E., Li, Z., Han, J., Luo, P.: Beyond one-to-one: Rethinking the referring image segmentation. In: Proceedings of the IEEE/CVF International Conference on Computer Vision. pp. 4067–4077 (2023) [3](#)
15. Jebur, M.N., Pradhan, B., Tehrany, M.S.: Optimization of landslide conditioning factors using very high-resolution airborne laser scanning (lidar) data at catchment scale. *Remote Sensing of Environment* **152**, 150–165 (2014) [2](#)
16. Kareem, A., Lahoud, J., Cholakkal, H.: Paris3d: Reasoning-based 3d part segmentation using large multimodal model. In: European Conference on Computer Vision. pp. 466–482. Springer (2024) [4](#)
17. Kirillov, A., Mintun, E., Ravi, N., Mao, H., Rolland, C., Gustafson, L., Xiao, T., Whitehead, S., Berg, A.C., Lo, W.Y., et al.: Segment anything. In: Proceedings of the IEEE/CVF international conference on computer vision. pp. 4015–4026 (2023) [8](#)
18. Kuckreja, K., Danish, M.S., Naseer, M., Das, A., Khan, S., Khan, F.S.: Geochat: Grounded large vision-language model for remote sensing. In: Proceedings of the IEEE/CVF Conference on Computer Vision and Pattern Recognition. pp. 27831–27840 (2024) [1](#), [3](#)
19. Labatie, A., Vaccaro, M., Lardiere, N., Garioud, A., Gonthier, N.: Maestro: masked autoencoders for multimodal, multitemporal, and multispectral earth observation data. In: Proceedings of the IEEE/CVF Winter Conference on Applications of Computer Vision. pp. 212–224 (2026) [5](#)
20. Lai, X., Tian, Z., Chen, Y., Li, Y., Yuan, Y., Liu, S., Jia, J.: Lisa: Reasoning segmentation via large language model. In: Proceedings of the IEEE/CVF Conference on Computer Vision and Pattern Recognition. pp. 9579–9589 (2024) [1](#), [2](#), [3](#), [8](#), [11](#)
21. Lane, K., Karimzadeh, M.: A genealogy of foundation models in remote sensing. *ACM Transactions on Spatial Algorithms and Systems* (2026) [3](#)
22. Li, K., Xin, Z., Pang, L., Pang, C., Deng, Y., Yao, J., Xia, G., Meng, D., Wang, Z., Cao, X.: Segearth-r1: Geospatial pixel reasoning via large language model. arXiv preprint arXiv:2504.09644 (2025) [3](#)
23. Li, X., Wen, C., Hu, Y., Yuan, Z., Zhu, X.X.: Vision-language models in remote sensing: Current progress and future trends. *IEEE Geoscience and Remote Sensing Magazine* **12**(2), 32–66 (2024) [2](#)
24. Liu, A.H., Khandelwal, K., Subramanian, S., Jouault, V., Rastogi, A., Sadé, A., Jeffares, A., Jiang, A., Cahill, A., Gavaudan, A., et al.: Ministral 3. arXiv preprint arXiv:2601.08584 (2026) [11](#)
25. Liu, B., Huang, Z., Li, Y., Gao, R., Chen, H.X., Xiang, T.Z.: Hatformer: Height-aware transformer for multimodal 3d change detection. *ISPRS Journal of Photogrammetry and Remote Sensing* **228**, 340–355 (2025) [4](#)
26. Liu, C., Ding, H., Jiang, X.: Gres: Generalized referring expression segmentation. In: Proceedings of the IEEE/CVF conference on computer vision and pattern recognition. pp. 23592–23601 (2023) [3](#)
27. Liu, H., Li, C., Li, Y., Lee, Y.J.: Improved baselines with visual instruction tuning. In: Proceedings of the IEEE/CVF conference on computer vision and pattern recognition. pp. 26296–26306 (2024) [1](#), [11](#)

28. Liu, H., Li, C., Li, Y., Li, B., Zhang, Y., Shen, S., Lee, Y.J.: Llvannext: Improved reasoning, ocr, and world knowledge (2024) [11](#)
29. Liu, H., Li, C., Wu, Q., Lee, Y.J.: Visual instruction tuning. *Advances in neural information processing systems* **36**, 34892–34916 (2023) [1](#)
30. Liu, Z., Mao, H., Wu, C.Y., Feichtenhofer, C., Darrell, T., Xie, S.: A convnet for the 2020s. In: *Proceedings of the IEEE/CVF conference on computer vision and pattern recognition*. pp. 11976–11986 (2022) [8](#)
31. Lobry, S., Marcos, D., Murray, J., Tuia, D.: Rsvqa: Visual question answering for remote sensing data. *IEEE Transactions on Geoscience and Remote Sensing* **58**(12), 8555–8566 (2020) [2](#), [7](#)
32. Milletari, F., Navab, N., Ahmadi, S.A.: V-net: Fully convolutional neural networks for volumetric medical image segmentation. In: *2016 fourth international conference on 3D vision (3DV)*. pp. 565–571. *Ieee* (2016) [10](#)
33. Quenum, J., Hsieh, W.H., Wu, T.H., Gupta, R., Darrell, T., Chan, D.M.: Lisat: Language-instructed segmentation assistant for satellite imagery. *arXiv preprint arXiv:2505.02829* (2025) [3](#)
34. Radford, A., Kim, J.W., Hallacy, C., Ramesh, A., Goh, G., Agarwal, S., Sastry, G., Askell, A., Mishkin, P., Clark, J., et al.: Learning transferable visual models from natural language supervision. In: *International conference on machine learning*. pp. 8748–8763. *PmLR* (2021) [8](#)
35. Ren, Z., Huang, Z., Wei, Y., Zhao, Y., Fu, D., Feng, J., Jin, X.: Pixellm: Pixel reasoning with large multimodal model. In: *Proceedings of the IEEE/CVF Conference on Computer Vision and Pattern Recognition*. pp. 26374–26383 (2024) [11](#)
36. Sampson, C.C., Smith, A.M., Bates, P.D., Neal, J.C., Alfieri, L., Freer, J.E.: A high-resolution global flood hazard model. *Water resources research* **51**(9), 7358–7381 (2015) [2](#)
37. Schumann, G., Bates, P.D., Apel, H., Aronica, G.T.: Global flood hazard mapping, modeling, and forecasting: Challenges and perspectives. *Global Flood Hazard: Applications in Modeling, Mapping, and Forecasting* pp. 239–244 (2018) [2](#)
38. Shabbir, A., Zumri, M., Bennamoun, M., Khan, F.S., Khan, S.: Geopixel: Pixel grounding large multimodal model in remote sensing. *arXiv preprint arXiv:2501.13925* (2025) [3](#)
39. Shu, Y., Ren, B., Xiong, Z., Pani Paudel, D., Van Gool, L., Demir, B., Sebe, N., Rota, P.: Earthmind: Towards multi-granular and multi-sensor earth observation with large multimodal models. *arXiv e-prints* pp. *arXiv-2506* (2025) [1](#)
40. Sun, Y., Feng, S., Li, X., Ye, Y., Kang, J., Huang, X.: Visual grounding in remote sensing images. In: *Proceedings of the 30th ACM International conference on Multimedia*. pp. 404–412 (2022) [2](#)
41. Sun, Z., Guo, P., Li, Z., Chen, X., Liu, X.: Elevation-aware domain adaptation for semantic segmentation of aerial images. *Remote Sensing* **17**(14), 2529 (2025) [4](#)
42. Tao, L., Zhang, H., Jing, H., Liu, Y., Yan, D., Wei, G., Xue, X.: Advancements in vision–language models for remote sensing: Datasets, capabilities, and enhancement techniques. *Remote Sensing* **17**(1), 162 (2025) [3](#)
43. Touvron, H., Martin, L., Stone, K., Albert, P., Almahairi, A., Babaei, Y., Bashlykov, N., Batra, S., Bhargava, P., Bhosale, S., et al.: Llama 2: Open foundation and fine-tuned chat models. *arXiv preprint arXiv:2307.09288* (2023) [6](#), [8](#)
44. Wang, R., Peethambaran, J., Chen, D.: Lidar point clouds to 3-d urban models : a review. *IEEE Journal of Selected Topics in Applied Earth Observations and Remote Sensing* **11**(2), 606–627 (2018) [2](#)

45. Wang, Y., Xiong, Z., Liu, C., Stewart, A.J., Dujardin, T., Bountos, N.I., Zavras, A., Gerken, F., Papoutsis, I., Leal-Taixé, L., et al.: Towards a unified copernicus foundation model for earth vision. arXiv preprint arXiv:2503.11849 (2025) [1](#)
46. Wang, Z., Prabha, R., Huang, T., Wu, J., Rajagopal, R.: Skyscript: A large and semantically diverse vision-language dataset for remote sensing. In: Proceedings of the AAAI Conference on Artificial Intelligence. vol. 38, pp. 5805–5813 (2024) [7](#)
47. Xia, Z., Han, D., Han, Y., Pan, X., Song, S., Huang, G.: Gsva: Generalized segmentation via multimodal large language models. In: Proceedings of the IEEE/CVF Conference on Computer Vision and Pattern Recognition. pp. 3858–3869 (2024) [3](#)
48. Xiao, A., Xuan, W., Wang, J., Huang, J., Tao, D., Lu, S., Yokoya, N.: Foundation models for remote sensing and earth observation: A survey. IEEE Geoscience and Remote Sensing Magazine (2025) [3](#)
49. Xin, Z., Li, K., Chen, L., Li, W., Xiao, Y., Qiao, H., Zhang, W., Meng, D., Cao, X.: Segearth-r2: Towards comprehensive language-guided segmentation for remote sensing images. arXiv preprint arXiv:2512.20013 (2025) [3](#)
50. Xiong, Z., Chen, S., Yi, W., Xiang, Z.: Parse semantics from geometry: A remote sensing benchmark for multi-modal semantic segmentation. Tech. Univ. Munich, Munich, Germany, Tech. Rep (2022) [5](#)
51. Xu, J., Jayakumar Nair, D., Waller, S.T.: Artificial intelligence in disaster management: achievements, challenges, and prospects. Natural Hazards pp. 1–57 (2025) [2](#)
52. Yang, A., Li, A., Yang, B., Zhang, B., Hui, B., Zheng, B., Yu, B., Gao, C., Huang, C., Lv, C., et al.: Qwen3 technical report. arXiv preprint arXiv:2505.09388 (2025) [11](#)
53. Zhang, W., Cai, M., Ning, Y., Zhang, T., Zhuang, Y., Chen, H., Li, J., Mao, X.: Earthgpt-x: Enabling mllms to flexibly and comprehensively understand multi-source remote sensing imagery. arXiv preprint arXiv:2504.12795 (2025) [3](#)
54. Zhang, W., Cai, M., Zhang, T., Zhuang, Y., Mao, X.: Earthgpt: A universal multimodal large language model for multisensor image comprehension in remote sensing domain. IEEE Transactions on Geoscience and Remote Sensing **62**, 1–20 (2024) [1](#), [3](#)
55. Zhang, Y., Ru, L., Wu, K., Yu, L., Liang, L., Li, Y., Chen, J.: Skysense v2: A unified foundation model for multi-modal remote sensing. In: Proceedings of the IEEE/CVF International Conference on Computer Vision. pp. 9136–9146 (2025) [3](#)
56. Zhang, Z., Shen, H., Zhao, T., Chen, B., Guan, Z., Wang, Y., Jia, X., Cai, Y., Shang, Y., Yin, J.: Georsmllm: A multimodal large language model for vision-language tasks in geoscience and remote sensing. arXiv preprint arXiv:2503.12490 (2025) [3](#)
57. Zheng, L., Chiang, W.L., Sheng, Y., Zhuang, S., Wu, Z., Zhuang, Y., Lin, Z., Li, Z., Li, D., Xing, E., et al.: Judging llm-as-a-judge with mt-bench and chatbot arena. Advances in neural information processing systems **36**, 46595–46623 (2023) [11](#)
58. Zhou, B., Yang, H., Chen, D., Ye, J., Bai, T., Yu, J., Zhang, S., Lin, D., He, C., Li, W.: Urbench: A comprehensive benchmark for evaluating large multimodal models in multi-view urban scenarios. In: Proceedings of the AAAI Conference on Artificial Intelligence. vol. 39, pp. 10707–10715 (2025) [2](#), [4](#)